
RGI : REGULARIZED GRAPH INFOMAX FOR SELF-SUPERVISED LEARNING ON GRAPHS

Oscar Pina

Technical University of Catalonia (UPC)
Barcelona, Spain
oscar.pina@upc.edu

Verónica Vilaplana

Technical University of Catalonia (UPC)
Barcelona, Spain
veronica.vilaplana@upc.edu

March 16, 2023

ABSTRACT

Self-supervised learning is gaining considerable attention as a solution to avoid the requirement of extensive annotations in representation learning on graphs. We introduce *Regularized Graph Infomax (RGI)*, a simple yet effective framework for node level self-supervised learning on graphs that trains a graph neural network encoder by maximizing the mutual information between node level local and global views, in contrast to previous works that employ graph level global views. The method promotes the predictability between views while regularizing the covariance matrices of the representations. Therefore, RGI is non-contrastive, does not depend on complex asymmetric architectures nor training tricks, is augmentation-free and does not rely on a two branch architecture. We run RGI on both transductive and inductive settings with popular graph benchmarks and show that it can achieve state-of-the-art performance regardless of its simplicity.

1 Introduction

The main goal of self-supervised learning is to learn useful representations of high-dimensional data without relying on annotations in order to leverage them in downstream tasks. Ideally, the obtained representations should be enough to efficiently fit other tasks with a small amount of labeled data.

In the vision domain, methods mainly focus on a maximization of the agreement between the representations of two views of an image. For instance, Deep InfoMax (DIM) [1] was initially proposed to maximize the mutual information (MI) between local and global views. However, methods based on data augmentation techniques have shown better performance. They are based on a two branch architecture, either symmetric or not, whose branches are fed with different augmented versions of an image obtained with random transformations such as rotation and cropping [2], [3], [4], [5], [6]. The encoder is trained to be invariant to those image distortions.

These schemes are also adopted for graph representation learning and successful algorithms have been extended to this domain [7], [8], [9], [10], [11], [12]. Consequently, graph specific data augmentation techniques are required to generate the graph views. Graph transformations can focus on both node attributes and the topology of the graph. Indeed, popular choices are node attribute masking and edge sampling [9], [10], [13], [11]. However, the idea behind invariance via data augmentations roots in the fact that it is assumed that these transformations do not change the semantics of the data and the information contained about the downstream task is kept. Whereas we can understand image augmentations, it is not clear how graph transformations modify its semantics nor if they can be applied to all graph domains [14]. To overcome this issue, graph diffusion has been proposed to create the alternative views [12], and other works attempt to get rid of the augmentations by designing strategies that leverage the local neighborhood of the nodes [15], [16], [17], also seen in concurrent work [18].

Additionally, the main challenge in multi-view scenarios is to avoid the collapse of the models, in which the encoder outputs constant representations for all inputs. Solutions can be divided into contrastive and non-contrastive. The former constructs positive and negative pairs and maximizes the similarity between components of the positive pairs while minimizing it for the elements of the negative pairs [4], [7], [1], [11], [12], [18]. However, it has been shown that

they require a large number of negative samples to efficiently work, which can be a bottleneck for scalability. Within non-contrastive methods, we can find, among others, knowledge distillation, which avoids the collapse by taking a teacher-student asymmetric architecture [5], [9], and regularized methods, which spread out embedded data points by regularizing the covariance matrix of the representations [2], [6], [10].

To cope with the aforementioned challenges, we introduce *RGI - Regularized Graph Infomax*, a simple yet effective self-supervised learning framework for graphs. The algorithm is augmentation-free, non-contrastive, and does not require a two-branch architecture nor complex training strategies. RGI trains an encoder maximizing the mutual information between nodes’ representations output by the model and their propagation through the graph, namely local and global views, respectively. The collapse is avoided with variance-covariance regularization loss terms that attempt to maximize the entropy of the representation space.

This paper is organized as follows, we first provide a background on mutual information (MI), the Infomax principle and the multi-view representation learning approach for images and graphs. Then, we formalize our algorithm RGI for self-supervised learning, provide intuitions behind the method and detail the objective function proposed. Then, we evaluate the method on multiple graph benchmark datasets and discuss the advantages of RGI with respect to other algorithms. The main contributions are listed below:

1. We derive a loss function that attempts to maximize the MI between two views of a node by relying on the reconstruction-based bound of the MI and regularizing the entropy of the representation space via the covariance matrix.
2. We define a node-level global view, particular to every node, as opposed to the graph-level view proposed in other methods [7], [8]. This is obtained by propagating the node representations through the graph and allows us to address one-to-one reconstruction.
3. We evaluate the algorithm on both transductive and inductive settings and show that, despite its simplicity, state-of-the-art performance is obtained in some of the benchmarks while being competitive in all of them. We also provide ablation studies on how the different designs of the method influence the performance, that demonstrate the robustness of RGI despite modifying core concepts of the algorithm.

2 Background

2.1 Information theory for representation learning

Mutual information The mutual information (MI) between two random variables X and Y , $I(X; Y)$ is a symmetric quantity, $I(X; Y) = I(Y; X)$, that measures how much information one variable carries about the other. Formally, it is defined as:

$$I(X; Y) = H(X) - H(X|Y) = H(Y) - H(Y|X) \quad (1)$$

where $H(X)$ is the entropy of X and $H(X|Y)$ is the conditional entropy of X given Y . This quantity can be lower-bounded by the expected reconstruction error, which is usually employed in generative models:

$$I(X; Y) = H(X) - H(X|Y) \geq H(X) - \mathcal{R}(X|Y) \quad (2)$$

where $\mathcal{R}(X|Y)$ is the expected reconstruction error of X given Y . In practice, this expected error is approximated with the square loss or the cross-entropy loss.

InfoMax principle The InfoMax principle [19] states that a neural network can be trained in a self-supervised manner by maximizing the mutual information between its input X and its output Y , $I(X; Y)$. To do so, [20] suggests that it is enough to maximize the entropy of Y , which, for the example of a one layer n-to-n network, is achieved by maximizing the logarithm of the jacobian of the weights. The intuition is that this quantity can be seen as the log of the volume space of Y onto which the values of X are mapped.

2.2 Multi-view representation learning

The InfoMax principle is extended to a multi-view approach, in which rather than maximizing the MI between the input and output of the network, the agreement is maximized between the representations of two different views of the input. This scenario has two main advantages, (i) the loss is computed in the representation space, which is in general lower dimensional and avoids focusing on small details of the input and (ii) views can be defined to capture different aspects of the data [21].

Local - global MI. Deep InfoMax [1] trains an encoder maximizing the average mutual information between local patches and global representations of an image. Deep Graph InfoMax [7] and InfoGraph [8] extend this work to the

graph domain, targetting the MI between node and graph level embeddings. The graph representation is obtained with a global pooling layer applied to the local node embeddings. In DGI, since most datasets consist of one single graph, the authors create a corrupted version of the graph by shuffling the node features and contrasting negative and positive pairs.

Invariance via data augmentation. SimCLR [4], BYOL [5], Barlow Twins [6] and VICReg [2], among others, create two augmented views of an image via data augmentation, such as image rotation and cropping, and train the encoder to be invariant to those augmentations, not necessarily with MI objectives. These works are also extended for self-supervised graph representation learning. For instance, GRACE [11] follows a similar approach to SimCLR based on contrastive learning, BGRL [9] employs the same asymmetric scheme than BYOL and G-BT, [13] directly extends Barlow Twins cross-covariance regularization objective.

2.3 Avoiding Collapse

Maximizing the agreement between views can lead to a total collapse in which the encoder outputs the same representation independently from the input. In order to diminish this phenomena, either architectural, regularization or training tricks can be employed:

Contrastive learning. Contrastive methods not only encourage the two views of the input (positive pairs) to be similar, but they also force views from different inputs (negative pairs) to be different [4], [7], [1], [11], [12], [18], [22], [14]. They have been successfully applied to all data domains, nonetheless, their performance is highly influenced by the number of negative pairs, usually requiring many of them to work efficiently.

Knowledge distillation. Knowledge distillation methods do not need negative pairs [5], [9]. Instead, they construct a teacher-student asymmetric architecture combined with a stop-gradient operation. Concretely, the networks are fed with two augmented views and the student network is trained to predict the output of the teacher model. Collapse is avoided by not backpropagating gradients through the teacher network to update its parameters, but setting them to be a moving average of the student’s parameters.

Covariance regularization. Covariance regularization consists of extending the loss function by including regularization terms on the covariance matrix of the representations, forcing high variances for every feature and low co-variances [2], [6], [10]. Under the gaussianity assumption, these loss terms attempt to regularize the entropy of the latent space to avoid the collapse [23].

3 Regularized Graph InfoMax

In this section, we detail our algorithm *RGI - Regularized Graph Infomax* for self-supervised learning on graphs.

Algorithm 1 RGI

```

1: Input: node features  $\mathbf{X}$ ; adjacency matrix  $\mathbf{A}$ ; parameters  $\Theta$ ,  $\phi$  and  $\psi$ ; backbone  $f_\Theta$ ; reconstruction networks  $h_\phi$ 
   and  $h_\psi$ ; propagation steps  $K$ .
2: repeat
3:    $\mathbf{U} = f_\Theta(\mathbf{X}, \mathbf{A})$  ▷ obtain local views
4:    $\mathbf{S} = \mathbf{D}^{-\frac{1}{2}} \mathbf{A} \mathbf{D}^{-\frac{1}{2}}$  ▷ get symmetric adjacency matrix
5:    $\mathbf{V} = \mathbf{S}^K \mathbf{U}$  ▷ propagate during K steps
6:    $\mathbf{V}' = h_\phi(\mathbf{U})$  ▷ reconstruction of  $V$  from  $U$ 
7:    $\mathbf{U}' = h_\psi(\mathbf{V})$  ▷ reconstruction of  $U$  from  $V$ 
8:    $\mathcal{C} = \frac{1}{N} \mathbf{U}^T \mathbf{U}$  ▷ covariance matrix of  $U$ 
9:    $\Sigma = \frac{1}{N} \mathbf{V}^T \mathbf{V}$  ▷ covariance matrix of  $V$ 
10:   $\mathcal{L}_1 = \|\mathbf{U} - \mathbf{U}'\|_F^2 + \|\mathbf{V} - \mathbf{V}'\|_F^2$  ▷ reconstruction loss
11:   $\mathcal{L}_2 = (1 - \text{diag}(\mathcal{C}))^2 + (1 - \text{diag}(\Sigma))^2$  ▷ variance loss
12:   $\mathcal{L}_3 = (\text{off-diag}(\mathcal{C}))^2 + (\text{off-diag}(\Sigma))^2$  ▷ covariance loss
13:   $\mathcal{L} = \lambda_1 \mathcal{L}_1 + \lambda_2 \mathcal{L}_2 + \lambda_3 \mathcal{L}_3$  ▷ loss function
14:   $\Theta, \phi, \psi \leftarrow \nabla_{\Theta, \phi, \psi} \mathcal{L}$  ▷ update parameters
15: until convergence
16: return  $\mathbf{U}$ 

```

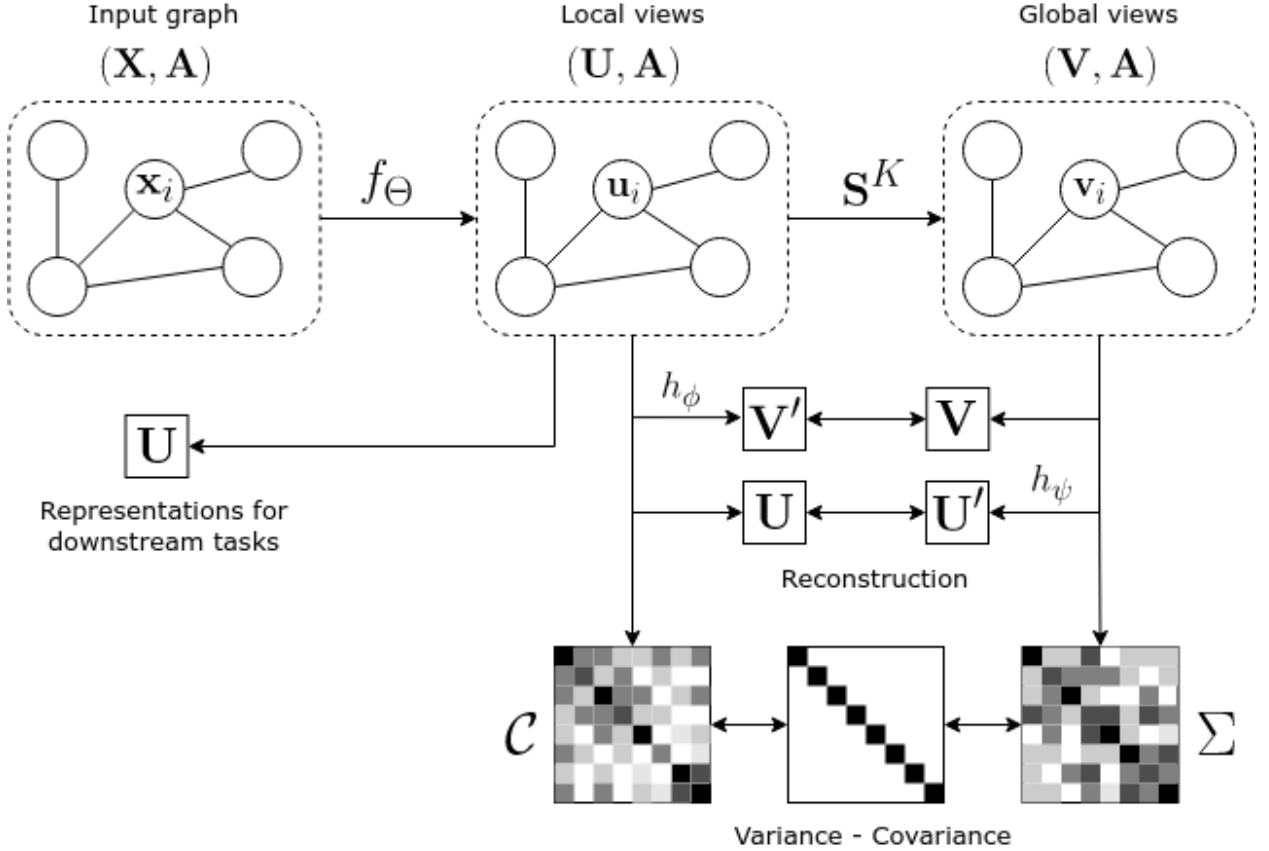


Figure 1: Visual illustration of RGI. Given the input graph $\mathcal{G} = (\mathbf{X}, \mathbf{A})$, a GNN encoder f_Θ extracts node features $\mathbf{U} = f_\Theta(\mathbf{X}, \mathbf{A})$ and they are propagated through the graph during K steps to obtain the nodes’ global views $\mathbf{V} = \mathbf{S}^K \mathbf{U}$. RGI maximizes the MI between \mathbf{U} and \mathbf{V} based on the lower bound of the MI of Equation 2. To do so, two auxiliary neural networks h_ϕ and h_ψ are trained to predict V from U and U from V , respectively. Additionally, the covariance matrices of the local and global views are regularized to have large diagonal elements and off-diagonal elements close to zero, attempting to maximize the entropy of \mathbf{U} and \mathbf{U} . The neural networks h_ϕ and h_ψ and the global views \mathbf{V} are ignored during inference.

3.1 Context and notation

Let $\mathcal{G} = (\mathcal{V}, \mathcal{E})$ be a graph of N nodes where \mathcal{V} is the node set and \mathcal{E} the edge set. Node attributes X come from d -dimensional empirical distribution, $X \sim \mathbb{P}_X$ and the nodes’ realizations are arranged in a matrix $\mathbf{X} = \{\mathbf{x}_i\}_{i=1}^N \in \mathbb{R}^{N \times d}$, where $\mathbf{x}_i \in \mathbb{R}^d$ are the attributes of node i . \mathcal{E} comes in the form of (unweighted) adjacency matrix $\mathbf{A} \in \{0, 1\}^{N \times N}$, $\mathbf{A}_{ij} = 1$ if the edge $e_{ij} \in \mathcal{E}$, 0 otherwise. The K -hop neighborhood of a node i , $\mathcal{G}_i^{(K)}$, is represented by the set of neighbors’ attributes, $\mathbf{X}_i^{(K)}$ and the induced adjacency matrix $\mathbf{A}_i^{(K)}$. The same notation criterion of X , \mathbf{X} , \mathbf{x}_i and \mathbf{X}_i will be employed for other node hidden representations.

The goal of graph self-supervised learning is to fit a graph neural network encoder $f_\Theta : \mathbb{R}^{N \times d} \times \{0, 1\}^{N \times N} \rightarrow \mathbb{R}^{N \times D}$, $\mathbf{U} = f_\Theta(\mathcal{G}) = f_\Theta(\mathbf{X}, \mathbf{A})$, parametrized by Θ , that obtains a D -dimensional vector representation \mathbf{u}_i for every node of the input graph \mathcal{G} without relying on node annotations.

3.2 Method

RGI trains an encoder to maximize the MI between local node views U and global ones V , arranged in matrices \mathbf{U} and \mathbf{V} , respectively. Local node views \mathbf{U} are the output of the L -layer graph neural network f_Θ to be trained, $\mathbf{U} = f_\Theta(\mathbf{X}, \mathbf{A})$. Global node views \mathbf{V} are obtained by propagating these representations through the graph during

K steps, $\mathbf{V} = g_K(\mathbf{U}, \mathbf{S}) = \mathbf{S}^K \mathbf{U}$, where \mathbf{S} is a graph shift operator such as the (normalized) adjacency matrix. The encoder is trained to output the representations \mathbf{U} that easily predict the representations after propagation and symmetrically predicting the output of the encoder from their propagation, while also including regularization on the covariance matrices of the local and global views, \mathcal{C} and Σ , respectively. The intuition is that given a node’s local view, one should be able to predict its global view, which better approximates the global position of the node on the graph. The local representations \mathbf{U} are then employed for downstream tasks. Two additional fully-connected neural networks h_ϕ, h_ψ are included during training for the reconstruction between views, but they are ignored for inference. The algorithm is described in Algorithm 1.

3.2.1 Local-global perspective

The node views \mathbf{V} are referenced as global views. This definition is different from the global pooling proposed in DGI [7], since the views are node level rather than graph level. This approach has the advantage of enabling addressing one-to-one reconstruction errors since every node has its own view.

The reason to call \mathbf{V} the global views is as follows. For a target node i , we obtain its local view with a L -layer GNN, $\mathbf{u}_i = f_\Theta(\mathbf{X}_i^{(L)}, \mathbf{A}_i^{(L)})$, so that it depends on its L -hop neighborhood. Afterwards, the global view is computed by propagating the representations through the graph during K steps, $\mathbf{v}_i = g_K(\mathbf{U}_i^{(K)}, \mathbf{A}_i^{(K)})$. Therefore, \mathbf{v}_i contains information of the $(L + K)$ -hop neighborhood of i . It is known that for a small-world network \mathcal{G} of N nodes, the diameter of the graph is $\text{diam}(\mathcal{G}) = \log(N)$. Consequently, in a small world network, \mathbf{v}_i can encode global information of every node in the graph as long as $L + K \simeq \log(N)$.

3.2.2 Loss function

The objective promotes the predictability between views, such that one view contains as much information as possible about the other. Additionally, we incorporate covariance matrix regularization terms to avoid the collapse of the representations [6], [2], [13], [10]. Being $\bar{\mathbf{U}}$ the mean-centered version of \mathbf{U} and $\mathcal{C} = \frac{1}{N} \bar{\mathbf{U}}^T \bar{\mathbf{U}}$ the covariance matrix, we define the loss:

$$\mathcal{L}_u = \frac{\lambda_1}{N} \sum_{i=1}^N \|\mathbf{u}_i - h_\phi(\mathbf{v}_i)\|_2^2 + \frac{\lambda_2}{D} \sum_{l=1}^D (1 - \mathcal{C}_{ll})^2 + \frac{\lambda_3}{D} \sum_{l=1}^D \sum_{k \neq l}^D \mathcal{C}_{lk}^2 \quad (3)$$

Where $\lambda_1, \lambda_2, \lambda_3 \in \mathbb{R}$ are weight hyperparameters. The first term of the equation is the expected prediction error of the node local views given the globals with a fully-connected neural network h_ϕ , whose parameters are also updated during training. The following two terms are regularization terms on the covariance matrix of the representations. Concretely, the former guides the diagonal elements (variances) to be close to one whereas the latter forces the non-diagonal elements (covariances) to be zero. Intuitively, maximizing the variance avoids the total collapse to a constant representation. On the other hand, covariance minimization encourages the encoder to leverage the whole capacity of the representation space rather than projecting the points to a lower dimensional subspace, also known as dimensional collapse [24]. Symmetrically, being $\bar{\mathbf{V}}$ the mean-centered version of \mathbf{V} and $\Sigma = \frac{1}{N} \bar{\mathbf{V}}^T \bar{\mathbf{V}}$ the covariance matrix of the global views, we define:

$$\mathcal{L}_v = \frac{\lambda_1}{N} \sum_{i=1}^N \|\mathbf{v}_i - h_\psi(\mathbf{u}_i)\|_2^2 + \frac{\lambda_2}{D} \sum_{l=1}^D (1 - \Sigma_{ll})^2 + \frac{\lambda_3}{D} \sum_{l=1}^D \sum_{k \neq l}^D \Sigma_{lk}^2 \quad (4)$$

The final loss of the method is the sum of \mathcal{L}_u and \mathcal{L}_v : $\mathcal{L} = \mathcal{L}_u + \mathcal{L}_v$.

4 Results and evaluation

We evaluate the quality of the node level representations output by our method on both transductive and inductive settings.

Datasets. For transductive learning we run RGI on 4 popular benchmarks: *Amazon Computers*, *Amazon Photos*, *Coauthor CS* and *Coauthor Physics*. Finally, inductive learning evaluation is addressed with the challenging *PPI* dataset. The statistics of the datasets are shown in Table 1.

Linear evaluation. We follow the linear evaluation protocol on graphs to assess the quality of the representations as proposed in [7]. It consists of first fitting a GNN encoder in a fully self-supervised manner, freezing the weights

Table 1: Statistics of the datasets employed in our experiments.

NAME	TASK	NUM. NODES	NUM. EDGES	NODE FEATURES	NUM. CLASSES
AMAZON COMPUTERS	TRANSDUCTIVE	13,752	245,861	767	10
AMAZON PHOTOS	TRANSDUCTIVE	7,650	119,081	745	8
COAUTHOR CS	TRANSDUCTIVE	18,333	81,894	6,805	15
COAUTHOR PHYSICS	TRANSDUCTIVE	34,493	247,962	8,415	5
PPI (24 GRAPHS)	INDUCTIVE	56,944	818,716	50	121 (MULTILABEL)

Table 2: Classification accuracies on transductive datasets averaged for 20 weight initializations.

METHOD	AM. COMPUTERS	AM. PHOTOS	Co. CS	Co. PHYSICS
RAW FT.	73.81 ± 0.00	78.53 ± 0.00	90.37 ± 0.00	93.58 ± 0.00
DEEPWALK	85.68 ± 0.06	89.44 ± 0.11	84.61 ± 0.22	91.77 ± 0.15
DEEPWALK + FEAT.	86.28 ± 0.07	90.05 ± 0.08	87.70 ± 0.04	94.90 ± 0.09
RANDOM-INIT	86.46 ± 0.38	92.08 ± 0.48	91.64 ± 0.29	93.71 ± 0.29
DGI [7]	83.95 ± 0.47	91.61 ± 0.22	92.15 ± 0.63	94.51 ± 0.52
GMI [15]	82.21 ± 0.31	90.68 ± 0.17	OOM	OOM
MVGRL [12]	87.52 ± 0.11	91.74 ± 0.07	92.11 ± 0.12	95.33 ± 0.03
GRACE [11]	89.53 ± 0.35	92.78 ± 0.45	91.12 ± 0.20	OOM
G-BT [13]	88.14 ± 0.33	92.63 ± 0.44	92.95 ± 0.17	95.07 ± 0.17
CCA-SSG [10]	88.74 ± 0.28	93.14 ± 0.14	93.31 ± 0.22	95.38 ± 0.06
BGRL [9]	90.34 ± 0.19	93.17 ± 0.30	93.31 ± 0.13	95.73 ± 0.05
AFGRL [16]	89.88 ± 0.37	93.22 ± 0.28	93.27 ± 0.17	95.69 ± 0.10
AFGCL [17]	89.68 ± 0.19	92.49 ± 0.31	91.92 ± 0.10	95.12 ± 0.15
LOCAL-GCL* [18]	88.81 ± 0.37	93.25 ± 0.40	94.90 ± 0.19	96.33 ± 0.13
PERTURBGCL* [22]	88.45 ± 0.77	93.62 ± 0.40	94.18 ± 0.09	95.85 ± 0.08
RGI (<i>ours</i>)	90.45 ± 0.08	92.94 ± 0.09	93.37 ± 0.07	95.91 ± 0.09

of the encoder, obtaining the node-level representations and fitting a linear classifier to a downstream task without backpropagating the gradients through the encoder. For comparability with other methods, the transductive settings are evaluated in terms of accuracy of the predictions whereas for the *PPI* dataset we employ the micro-average F1-score. As usual, since there is no public split for these datasets, *Amazon Computers*, *Amazon Photos*, *Coauthor CS* and *Coauthor Physics* are randomly split into train/validation/test (10% / 10% / 80%). To evaluate on the *PPI* dataset, we employ the standard pre-defined split, which has 20 graphs to fit the model, 2 graphs for validation and another two for testing.

4.1 Transductive learning

Architecture. As in [7], [9], among others, we fix the encoder f_{Θ} to be a $L = 2$ layer GCN [25]. We have set the output dimensionality to be 512 for all datasets and the hidden, 1024. We include batch normalization [26] and ReLU activation after the first layer but none of them is included after the second convolutional layer. Therefore, if $\hat{\mathbf{A}} = \mathbf{A} + \mathbf{I}$, and $\hat{\mathbf{A}}_n = \hat{\mathbf{D}}^{-\frac{1}{2}} \hat{\mathbf{A}} \hat{\mathbf{D}}^{-\frac{1}{2}}$ the matrix equation of the encoder is:

$$\mathbf{Z} = \hat{\mathbf{A}}_n \left[\text{ReLU} \left(\text{BN} \left(\hat{\mathbf{A}}_n \mathbf{X} \mathbf{W}_1 \right) \right) \right] \mathbf{W}_2 \quad (5)$$

The node global views are obtained by propagating the node local views output by the encoder. We employ the normalized adjacency matrix as shift operator $\mathbf{S} = \mathbf{D}^{-\frac{1}{2}} \mathbf{A} \mathbf{D}^{-\frac{1}{2}}$ without self-loops and propagate for $K = 1$ step. The networks h_{ϕ} and h_{ψ} are implemented with a two layer FCNN and ReLU activation in the hidden layer. However, no batch normalization is employed for these reconstruction networks.

Numerical results. Table 2 shows the mean accuracy of the linear evaluation protocol on the transductive graph settings. Our results are the average of 20 model weight initializations and data splits. The other results are extracted from previous reports. We can observe that RGI performs competitively in all datasets despite its simplicity and achieves state of the art in some of them. In except of *Amazon Computers* dataset, RGI is trained for 1,000 epochs whereas other

Table 3: Classification micro-average F1 score on PPI dataset averaged for 20 weight initializations.

METHOD	PPI
RAW FT.	42.20
RDM-INIT	62.60 \pm 0.20
DGI [7]	63.80 \pm 0.20
GMI [15]	65.00 \pm 0.02
GRACE [11]	69.71 \pm 0.17
G-BT [13]	70.49 \pm 0.19
BGRL [9]	70.49 \pm 0.05
RGI (<i>ours</i>)	72.16 \pm 0.11

Table 4: Effect of loss symmetrization. Linear evaluation accuracy (micro-average F-Score for PPI dataset) after fitting and encoder with different self-supervised objective functions averaged for 5 weight initializations and data splits.

\mathcal{L}	AM. COMPUTERS	AM. PHOTOS	CO. CS	CO. PHYSICS	PPI (F-SCORE)
\mathcal{L}_u	90.37 \pm 0.08	92.09 \pm 0.18	93.37 \pm 0.08	95.92 \pm 0.05	72.09 \pm 0.12
\mathcal{L}_v	90.52 \pm 0.09	92.86 \pm 0.07	93.36 \pm 0.05	95.93 \pm 0.04	70.44 \pm 0.12
$\mathcal{L}_u + \mathcal{L}_v$	90.45 \pm 0.07	92.88 \pm 0.13	93.37 \pm 0.03	95.93 \pm 0.04	72.25 \pm 0.09

methods such as BGRL require 10,000 epochs [9]. [13] reports the results of BGRL if training during 1,000 epochs, which imply a drop in performance in all datasets.

Regularizing with dropout. Albeit not crucial, we have found it useful to add noise to the input graph to regularize the learning procedure. Concretely, we can apply dropout and edge sampling before feeding the graph neural network with the graph. However, as discussed in Section 5, this approach is different to invariance via data augmentation, since the only purpose of these corruptions is regularization and no invariance assumption is made. We have applied standard dropout to the node features and edge sampling to the input graph with a probability of $p_{input} = 0.5$.

4.2 Inductive learning

Architecture. Based on previous reports [13], [9], we implement the encoder with a $L = 3$ layer GAT [27] with ELU activation and skip connections. Both hidden and output dimensionality are set to 512. Although a mean-pooling scheme would be more appropriate for inductive settings [28], we also employ the normalized adjacency matrix as graph shift operator to obtain the global views, $\mathbf{S} = \mathbf{D}^{-\frac{1}{2}} \mathbf{A} \mathbf{D}^{-\frac{1}{2}}$, and propagate for $K = 1$ steps. In Section 4.3.2 we study the effect of \mathbf{S} and K . The reconstruction networks h_ϕ and h_ψ have the same architecture as in the transductive setting.

Numerical results. Table 3 shows the micro-average F1-score of the linear evaluation averaged for 20 runs. RGI outperforms the current state of the art on this challenging dataset and only requires 2,000 epochs to reach this performance.

Sparse node features. PPI node features are sparse, with around 40% of empty features, which makes neighborhood aggregation crucial for any downstream node level task. Consequently, in order to experiment with dropout regularization, we have applied the dropout and edge sampling after the GNN encoder with a probability $p_{local} = 0.5$ and no dropout applied to the input $p_{input} = 0$.

4.3 Ablations

In this section, we run an ablation analysis to evaluate the effect of the two main components of the design space of RGI: the loss function \mathcal{L} and the global propagation scheme, which includes the shift operator \mathbf{S} and the number of propagation steps K . In addition, we have experimented with the dropout regularization. Generally, results show that RGI performs robustly for different design configurations, specifically in transductive settings.

Table 5: Effect of global propagation scheme. Linear evaluation accuracy (micro-average F-Score for PPI dataset) for different schemes to obtain the global views propagating the local ones averaged for 5 weight initializations and data splits.

S	K	AM. COMPUTERS	AM. PHOTOS	Co. CS	Co. PHYSICS	PPI (F-SCORE)
$\mathbf{D}^{-1}\mathbf{A}$	1	90.52 \pm 0.09	92.81 \pm 0.14	93.39 \pm 0.04	95.89 \pm 0.07	71.29 \pm 0.11
$\mathbf{D}^{-1}\mathbf{A}$	2	90.43 \pm 0.16	92.84 \pm 0.15	93.37 \pm 0.04	95.89 \pm 0.07	71.28 \pm 0.08
$\mathbf{D}^{-1}\mathbf{A}$	5	90.41 \pm 0.17	92.84 \pm 0.08	93.26 \pm 0.06	95.86 \pm 0.08	70.06 \pm 0.08
$\mathbf{D}^{-\frac{1}{2}}\mathbf{A}\mathbf{D}^{-\frac{1}{2}}$	1	90.46 \pm 0.06	92.89 \pm 0.15	93.37 \pm 0.02	95.92 \pm 0.04	72.25 \pm 0.13
$\mathbf{D}^{-\frac{1}{2}}\mathbf{A}\mathbf{D}^{-\frac{1}{2}}$	2	90.25 \pm 0.10	92.69 \pm 0.14	93.35 \pm 0.02	95.91 \pm 0.04	71.94 \pm 0.08
$\mathbf{D}^{-\frac{1}{2}}\mathbf{A}\mathbf{D}^{-\frac{1}{2}}$	5	90.08 \pm 0.16	92.75 \pm 0.11	93.23 \pm 0.05	95.85 \pm 0.05	70.08 \pm 0.17
$\mathbf{I} - \mathbf{D}^{-\frac{1}{2}}\mathbf{A}\mathbf{D}^{-\frac{1}{2}}$	1	84.22 \pm 0.28	90.23 \pm 0.20	93.01 \pm 0.12	95.50 \pm 0.11	61.81 \pm 0.08
$\mathbf{I} - \mathbf{D}^{-\frac{1}{2}}\mathbf{A}\mathbf{D}^{-\frac{1}{2}}$	2	84.58 \pm 0.22	90.75 \pm 0.25	92.89 \pm 0.14	95.46 \pm 0.08	61.35 \pm 0.13
$\mathbf{I} - \mathbf{D}^{-\frac{1}{2}}\mathbf{A}\mathbf{D}^{-\frac{1}{2}}$	5	88.65 \pm 0.16	92.62 \pm 0.20	91.82 \pm 0.27	95.53 \pm 0.09	64.5 \pm 0.12

Table 6: Effect of dropout and edge sampling regularization. Linear evaluation accuracy (micro-average F-Score for PPI dataset) for different values of dropout and edge sampling probabilities applied to the input graph before the GNN encoder (p_{input}) or to the local views before the propagation through the graph (p_{local}).

p_{input}	p_{output}	AM. COMPUTERS	AM. PHOTOS	Co. CS	Co. PHYSICS	PPI (F-SCORE)
0.0	0.0	89.89 \pm 0.09	92.66 \pm 0.16	93.41 \pm 0.03	95.93 \pm 0.03	71.36 \pm 0.14
0.0	0.5	90.00 \pm 0.16	92.85 \pm 0.14	93.32 \pm 0.04	95.88 \pm 0.05	72.25 \pm 0.09
0.5	0.0	90.45 \pm 0.07	92.90 \pm 0.13	93.37 \pm 0.03	95.92 \pm 0.04	67.98 \pm 0.21
0.5	0.5	90.34 \pm 0.08	92.99 \pm 0.17	93.30 \pm 0.06	95.88 \pm 0.05	67.96 \pm 0.07

4.3.1 Loss function

The loss function \mathcal{L} is symmetrized by applying covariance regularization to both local and global views and computing the reconstruction error on both sides. In this section, we empirically evaluate the effect of this symmetrization by training RGI with three different objectives: \mathcal{L}_u , \mathcal{L}_v and $\mathcal{L}_u + \mathcal{L}_v$. Section 4 shows a performance comparison on all transductive and inductive datasets we have experimented with. Note that the metrics do not match the reported ones since in the ablations we are only averaging for 5 weights initializations and data splits. Results suggest that, in full graph transductive settings, there is no need to symmetrize the loss function and targeting either \mathcal{L}_u or \mathcal{L}_v is enough since the performance is statistically similar. Indeed, targeting \mathcal{L}_v also influences the variance and covariance of the local views. Nonetheless, in PPI dataset, we can observe that \mathcal{L}_v objective alone does not lead to state-of-the-art performance since the variance and covariance of the local views is not influenced as in the transductive settings due to the batched, inductive nature of the problem. In general, although it may be tuned given the downstream task, $\mathcal{L}_u + \mathcal{L}_v$ performs competitively in all settings.

4.3.2 Global propagation scheme

The global views are obtained by propagating the output of the encoder during K steps with a graph shift operator \mathbf{S} , $\mathbf{V} = \mathbf{S}^K \mathbf{U}$. In this section, we evaluate different shifts operators, namely the mean-propagation $\mathbf{S} = \mathbf{D}^{-1}\mathbf{A}$, the normalized adjacency matrix $\mathbf{S} = \mathbf{D}^{-\frac{1}{2}}\mathbf{A}\mathbf{D}^{-\frac{1}{2}}$ and the normalized Laplacian $\mathbf{S} = \mathbf{I} - \mathbf{D}^{-\frac{1}{2}}\mathbf{A}\mathbf{D}^{-\frac{1}{2}}$ as well as different values of K , 1, 2 and 5. Note that none of them include the self-loops as opposed to most GNN propagation schemes. Section 5 shows that RGI performs robustly in all settings as long as the global propagation scheme captures the low-frequency components of the data, obtained with the adjacency matrix (either mean pooling or normalized), which is motivated by the homophily of the downstream task on the graph.

4.3.3 Dropout regularization

RGI can optionally include dropout and edge sampling regularization that can be applied to the input graph or to the graph before computing the global views. Section 6 shows the performance with four different configurations, where the columns *input* and *local* are the probabilities of dropout and edge sampling to the input graph and to the graph with local views, respectively. As it is argued in Section 5, these corruptions act as regularization rather than data

augmentation to seek invariance. The influence of the regularization on the transductive settings is minimal, whereas it boosts the performance in the batched inductive setting.

5 Discussion

We have presented an algorithm that achieves state-of-the-art performance even though it is much simpler in terms of theoretical interpretation, architecture and training strategy than other methods. In this section, we detail aspects of RGI and its advantages with respect to other methods.

Augmentation-free. Most previous works train an encoder with the invariance via data augmentation principle [9], [11], [10], [12], [14], [15]. It has been stated that transformations that drop information may modify the semantics of the graph so the invariance assumption may be incorrect and not hold for all graph domains. Other works propose alternative views leveraging the rich structure of graph data [12], [14], [15], [16], [17], but they also require carefully designed strategies to obtain the views. Alternatively, more recent methods also propose augmentation-free solutions [18], [17] by incorporating training tricks. RGI falls into this category and require no transformations, however, it is much more intuitive and only involves graph convolution-like operations.

Non-contrastive. Graph contrastive learning is the most popular approach to avoid the collapse of the representations by relying on negative pair sampling [7], [8], [11], [14], [17]. BGRL [9] and CCA-SSG [10], instead, do not need negative samples. The former avoids collapse with an asymmetric architecture and the later, regularizing the covariance matrix of the representations. In this work, we also adopt a regularized solution since it is more interpretable and naturally avoids the collapse whereas it is still an open problem to theoretically demonstrate that bootstrapped methods avoid trivial solutions.

Single branch architecture. Current state of the art algorithms usually rely on a joint embedding architecture that require multiple forward passes at each training step. For example, BGRL [9] forwards the graph through the encoder four times at each iteration. On the contrary, RGI is much more efficient and only performs one single forward pass while achieving similar performance to BGLR and other methods.

Dropout regularization. Optionally, RGI can add noise to the input graph for example with dropout and edge sampling. However, this noise acts as regularization rather than data augmentation. First, we do not train the encoder to be invariant to these transformations since we only compute one forward pass. Secondly, no invariance is assumed, the loss function does not include any term to make the encoder invariant to the transformations, instead, we compute the iterations with noisy versions of the graph. Finally, node attribute masking transformation usually drops the same feature for all nodes of the graph whereas we are employing standard dropout on the input features.

6 Conclusions

In this work we have introduced RGI, a simple yet effective framework for self-supervised learning on graphs based on the principle of mutual information maximization between local and global representations. The objective function regularizes the covariance matrix of the representations to avoid the total and dimensional collapse. We have shown that, in spite of its simplicity and that it does not require training for too long, it achieves state-of-the-art performance on multiple datasets following the linear evaluation protocol on downstream tasks.

References

- [1] R Devon Hjelm, Alex Fedorov, Samuel Lavoie-Marchildon, Karan Grewal, Phil Bachman, Adam Trischler, and Yoshua Bengio. Learning deep representations by mutual information estimation and maximization. In *International Conference on Learning Representations*, 2019.
- [2] Adrien Bardes, Jean Ponce, and Yann LeCun. Vicreg: Variance-invariance-covariance regularization for self-supervised learning. In *ICLR*, 2022.
- [3] Ting Chen, Simon Kornblith, Kevin Swersky, Mohammad Norouzi, and Geoffrey Hinton. Big self-supervised models are strong semi-supervised learners. *arXiv preprint arXiv:2006.10029*, 2020.
- [4] Ting Chen, Simon Kornblith, Mohammad Norouzi, and Geoffrey Hinton. A simple framework for contrastive learning of visual representations. *arXiv preprint arXiv:2002.05709*, 2020.
- [5] Jean-Bastien Grill, Florian Strub, Florent Altché, Corentin Tallec, Pierre H. Richemond, Elena Buchatskaya, Carl Doersch, Bernardo Avila Pires, Zhaohan Daniel Guo, Mohammad Gheshlaghi Azar, Bilal Piot, Koray

- Kavukcuoglu, Rémi Munos, and Michal Valko. Bootstrap your own latent: A new approach to self-supervised learning, 2020.
- [6] Jure Zbontar, Li Jing, Ishan Misra, Yann LeCun, and Stéphane Deny. Barlow twins: Self-supervised learning via redundancy reduction. *arXiv preprint arXiv:2103.03230*, 2021.
- [7] Petar Veličković, William Fedus, William L. Hamilton, Pietro Liò, Yoshua Bengio, and R Devon Hjelm. Deep Graph Infomax. In *International Conference on Learning Representations*, 2019.
- [8] Fan-Yun Sun, Jordan Hoffman, Vikas Verma, and Jian Tang. Infograph: Unsupervised and semi-supervised graph-level representation learning via mutual information maximization. In *International Conference on Learning Representations*, 2019.
- [9] Shantanu Thakoor, Corentin Tallec, Mohammad Gheshlaghi Azar, Mehdi Azabou, Eva L. Dyer, Rémi Munos, Petar Veličković, and Michal Valko. Large-scale representation learning on graphs via bootstrapping, 2021.
- [10] Hengrui Zhang, Qitian Wu, Junchi Yan, David Wipf, and S Yu Philip. From canonical correlation analysis to self-supervised graph neural networks. In *Thirty-Fifth Conference on Neural Information Processing Systems*, 2021.
- [11] Yanqiao Zhu, Yichen Xu, Feng Yu, Qiang Liu, Shu Wu, and Liang Wang. Deep Graph Contrastive Representation Learning. In *ICML Workshop on Graph Representation Learning and Beyond*, 2020.
- [12] Kaveh Hassani and Amir Hosein Khasahmadi. Contrastive multi-view representation learning on graphs. In *Proceedings of International Conference on Machine Learning*, pages 3451–3461. 2020.
- [13] Piotr Bielak, Tomasz Kajdanowicz, and Nitesh V. Chawla. Graph barlow twins: A self-supervised representation learning framework for graphs, 2021.
- [14] Dongkuan Xu, Wei Cheng, Dongsheng Luo, Haifeng Chen, and Xiang Zhang. Infogcl: Information-aware graph contrastive learning. In M. Ranzato, A. Beygelzimer, Y. Dauphin, P.S. Liang, and J. Wortman Vaughan, editors, *Advances in Neural Information Processing Systems*, volume 34, pages 30414–30425. Curran Associates, Inc., 2021.
- [15] Zhen Peng, Wenbing Huang, Minnan Luo, Qinghua Zheng, Yu Rong, Tingyang Xu, and Junzhou Huang. Graph Representation Learning via Graphical Mutual Information Maximization. In *Proceedings of The Web Conference*, 2020.
- [16] Namkyeong Lee, Junseok Lee, and Chanyoung Park. Augmentation-free self-supervised learning on graphs. 2022.
- [17] Haonan Wang, Jieyu Zhang, Qi Zhu, and Wei Huang. Augmentation-free graph contrastive learning with performance guarantee, 2022.
- [18] Anonymous. Localized graph contrastive learning. In *Submitted to The Eleventh International Conference on Learning Representations*, 2023. under review.
- [19] R. Linsker. Self-organization in a perceptual network. *Computer*, 21(3):105–117, 1988.
- [20] A J Bell and T J Sejnowski. An information-maximization approach to blind separation and blind deconvolution. *Neural Comput*, 7(6):1129–1159, November 1995.
- [21] Michael Tschannen, Josip Djolonga, Paul K. Rubenstein, Sylvain Gelly, and Mario Lucic. On mutual information maximization for representation learning. In *International Conference on Learning Representations*, 2020.
- [22] Anonymous. Graph contrastive learning with model perturbation. In *Submitted to The Eleventh International Conference on Learning Representations*, 2023. under review.
- [23] Ravid Shwartz-Ziv, Randall Balestriero, and Yann LeCun. What do we maximize in self-supervised learning?, 2022.
- [24] Tianyu Hua, Wenxiao Wang, Zihui Xue, Yue Wang, Sucheng Ren, and Hang Zhao. On feature decorrelation in self-supervised learning. *arXiv e-prints*, pages arXiv–2105, 2021.
- [25] Thomas N. Kipf and Max Welling. Semi-supervised classification with graph convolutional networks. In *International Conference on Learning Representations*, 2017.
- [26] Sergey Ioffe and Christian Szegedy. Batch normalization: Accelerating deep network training by reducing internal covariate shift. In *Proceedings of the 32nd International Conference on International Conference on Machine Learning - Volume 37, ICML'15*, page 448–456. JMLR.org, 2015.
- [27] Petar Veličković, Guillem Cucurull, Arantxa Casanova, Adriana Romero, Pietro Liò, and Yoshua Bengio. Graph attention networks. In *International Conference on Learning Representations*, 2018.

- [28] Will Hamilton, Zhitao Ying, and Jure Leskovec. Inductive representation learning on large graphs. In I. Guyon, U. Von Luxburg, S. Bengio, H. Wallach, R. Fergus, S. Vishwanathan, and R. Garnett, editors, *Advances in Neural Information Processing Systems*, volume 30. Curran Associates, Inc., 2017.